Stable trajectory planning and energy-efficience control allocation of lane change maneuver for autonomous electric vehicle

Liwei Xu and Guodong Yin
School of Mechanical Engineering, Southeast University, Nanjing, China
Guangmin Li
Southeast University, Nanjing, China
Athar Hanif
Department of Electrical Engineering, COMSATS Institute of Information Technology, Lahore, Pakistan, and
Chentong Bian
Southeast University, Nanjing, China

Abstract

Purpose – The purpose of this paper is to investigate problems in performing stable lane changes and to find a solution to reduce energy consumption of autonomous electric vehicles.

Design/methodology/approach – An optimization algorithm, model predictive control (MPC) and Karush–Kuhn–Tucker (KKT) conditions are adopted to resolve the problems of obtaining optimal lane time, tracking dynamic reference and energy-efficient allocation. In this paper, the dynamic constraints of vehicles during lane change are first established based on the longitudinal and lateral force coupling characteristics and the nominal reference trajectory. Then, by optimizing the lane change time, the yaw rate and lateral acceleration that connect with the lane change time are limed. Furthermore, to assure the dynamic properties of autonomous vehicles, the real system inputs under the restraints are obtained by using the MPC method. Based on the gained inputs and the efficient map of brushless direct-current in-wheel motors (BLDC IWMs), the nonlinear cost function which combines vehicle dynamic and energy consumption is given and the KKT-based method is adopted.

Findings – The effectiveness of the proposed control system is verified by numerical simulations. Consequently, the proposed control system can successfully achieve stable trajectory planning, which means that the yaw rate and longitudinal and lateral acceleration of vehicle are within stability boundaries, which accomplishes accurate tracking control and decreases obvious energy consumption.

Originality/value – This paper proposes a solution to simultaneously satisfy stable lane change maneuvering and reduction of energy consumption for autonomous electric vehicles. Different from previous path planning researches in which only the geometric constraints are involved, this paper considers vehicle dynamics, and stability boundaries are established in path planning to ensure the feasibility of the generated reference path.

Keywords Autonomous electric vehicle, Energy-efficient control allocation, Lane change maneuver, Stable trajectory planning

Paper type Research paper

1. Introduction

Autonomous vehicles (AV) and electric vehicles (EV), wherein in-wheel motors (IWMs) are adopted to drive wheels, have attracted increasing attention from both industrial and academic communities recently. Autonomous driving technology has tremendous potential in reducing vehicle casualties, and IWM EV can immensely enhance energy efficiency and lead to flexibility actuation which considerably enhances vehicle maneuverability, stability and safety (Li *et al.*, 2013; Jin *et al.*, 2015; Yin *et al.*, 2015). Numerous studies have revealed that A-IWM EV is an effective option that can increase

The current issue and full text archive of this journal is available on Emerald Insight at: **www.emeraldinsight.com/2399-9802.htm**

Journal of Intelligent and Connected Vehicles
1/2 (2018) 55–65
Emerald Publishing Limited [ISSN 2399-9802]
[DOI 10.1108/JICV-12-2017-0002]

This work was supported by the National Key R&D Program in China with grant 2016YFB0100906, National Key R&D Program in China with grant 2016YFD0700905, National Natural Science Foundation of China (No. 51575103), National Natural Science Foundation of China-Automotive joint fund (No. U1664258), Six Talent Peaks Project in Jiangsu Province (No. 2014-JXQC-001), Qing Lan Project and the Fundamental Research Funds for the Central Universities (2242016K41056) and the Scientific Research Foundation of Graduate School of Southeast University and Southeast University Excellent Doctor Degree Thesis Training Fund (No. YBJJ1704).

Received 31 December 2017
Revised 21 March 2018
30 April 2018
1 June 2018
Accepted 13 June 2018

traffic safety and decrease emissions and energy crisis (Li *et al.*, 2017; Potluri and Singh, 2015).

Unlike manned vehicles, which follow the driver's command to accomplish various driving tasks with the result that driver characteristics, vehicle dynamic features and energy management are major concerns (Wang *et al.*, 2013, 2015, 2016; Wu *et al.*, 2013; Dai *et al.*, 2014), the AV is supposed to appropriately perform various maneuvers under rare driver interventions or even without drivers. Therefore, autonomous lane change and the corresponding abilities of trajectory planning and trajectory tracking are most significant for AV. Many research works have been conducted in lane-changing trajectory planning (Soudbakhsh *et al.*, 2013; Kim *et al.*, 2014; Chen *et al.*, 2014; You *et al.*, 2015) and lane change control (Bayar, 2013; Berntorp *et al.*, 2014; Naranjo *et al.*, 2008). For example, Soudbakhsh *et al.* (2013) evaluated three different path planning methods – state lattice, predictive constraint-based planning and spline-based search tree. Chen *et al.* (2014) proposed a feasible trajectory generation algorithm based on quartic Be¨zier curve to generate local trajectory for AV. You *et al.* (2015) adopted a polynomial method to describe the trajectory of AV carrying out the lane change maneuver. In comparison to conventional path planning strategies (such as road map, cell decomposition and potential field methods), which are constantly mentioned in the robotics field, the above curve-type path planning methods can greatly reduce calculation and avoid being stuck in the local minima. For lane change control, Bayar (2013) used the PID method to resolve the trajectory tracking control. In Berntorp *et al.* (2014), an optimal trajectory-based minimization of yaw acceleration was acquired, and the simulation and comparative analysis were done with different speed values. In Naranjo *et al.* (2008), the fuzzy controllers that mimicked human behavior and reactions were established to conduct AV executing the overtaking maneuver in the scenario of two vehicles overtaking.

Although the above research works on lane change path planning and lane change control have made great contributions, there are still some apparent shortages that need to be settled. To begin with, current researches about lane change trajectory planning only consider geometric constraints and kinematic characteristics (e.g. the road curvature and lateral acceleration); the restrictions associated with vehicle dynamic characteristics are normally neglected. Consequently, the vehicle's dynamic stability may not be fulfilled if the AV drives along the predesigned trajectory. In addition, the problem of the A-IWM EV's energy efficiency during lane change is rarely considered. For EV, especially for A-IWM EV, despite the redundant degrees of freedom providing additional control flexibility in maintaining vehicle safety and stability (such as Traction Control and Direct Yaw Control), unreasonable dynamic control laws that ignore the energy consumption may immensely shorten the driving mileage of EV.

Based on the aforementioned discussion, this paper presents a novel lane change control system for A-IWM EV, which consists of a stable trajectory planning level that ensures the feasibility of the generated reference path, a high-level model predictive control (MPC) and a low-level energy-efficient control allocation (EECA) scheme, to enhance the feasibility of lane changing and to reduce energy expenditure. The rest of this paper is organized as follows. In Section 2, the stable lane change trajectory that includes vehicle constraints is developed. A control-oriented model of IWM EV planar motion is described in Section 3. In Section 4, the control system is proposed. In Section 5, simulation results are displayed to verify the control performance and energy savings of the EECA. Conclusion is presented in Section 6.

2. Stable lane change trajectory

In this section, a new lane change trajectory that can guarantee the stability of A-IMW EV and keep the vehicle running smoothly is proposed. To establish this trajectory, the fifth-order polynomial function is first used to realize smooth lane change and the maximal comfortableness of passenger. Then, by founding the rational vehicle stability bounds and introducing those constraints into the trajectory equations, the stable lane change trajectory is created.

It should be noticed that in this paper, only the scenario of active lane change is considered, i.e. there should be no vehicles in the front and target lanes when the A-IMW EV is changing lanes. Therefore, the situation of collection avoidance is not considered in the reference trajectory generation. The corresponding path planning that can guarantee the stability of the vehicle and prevent vehicle collision at the same time can be studied in future research.

2.1 Stability constraints of in-wheel motors and electric vehicles

This section describes the plane dynamics of IMW EV. Hence, the stability constraints on longitudinal movement, lateral movement and yaw movement are constructed. In light of the vehicle dynamics, the lateral acceleration can be expressed as:

$$a_y = \omega v_x + \dot{v}_y \tag{1}$$

where ω is the yaw rate, v_x and v_y are the longitudinal and lateral velocities. Denoting β the slip angle of Center of Mass (CM), we get $v_y = v_x \tan(\beta)$. The relationship between the lateral acceleration, yaw rate and slip angle can be described as follows:

$$a_y = \omega v_x + \tan\beta \dot{v}_x + \frac{\dot{\beta} v_x}{\sqrt{1+\tan^2\beta}} \tag{2}$$

Note that the lateral acceleration should not exceed the maximal force that the ground can offer. Suppose β and β are small during vehicle lane change, the yaw rate of the vehicle under steady state should meet the following constraints (Rajamani, 2011):

$$|\omega| \le \frac{\varepsilon \mu g}{v_x} \tag{3}$$

where μ is the adhesion coefficient, g is the gravity coefficient and ε is the scale factor, which is usually approximately equal to 0.85 in practical calculation. In addition, because the linear tire model is used in this paper, the maximum lateral acceleration should not surpass 0.5g to ensure the tire working in the linear area, i.e.

$$|a_y| \le 0.5g \tag{4}$$

Thus equation (3) is modified as:

$$|\omega| \le \frac{0.5\varepsilon\mu g}{v_x} \tag{5}$$

For longitudinal acceleration a_x, according to the adhere-circle restriction, as shown in Figure 1, the longitudinal acceleration should abide by the following inequality:

$$|a_x| \le \sqrt{\mu^2 g^2 - 0.25g^2} \tag{6}$$

2.2 Reference trajectory generation

Assume t_0 is the initial time of lane change, t_f is the window time of lane change and the initial and final lateral states of the vehicle during lane change are $[Y_0, v_{y0}, a_{y0}]^T$ and $[Y_f, v_{yf}, a_{yf}]^T$. Hypothetically, if the vehicle carries out straight line driving before and after lane change, then $a_{y0} = v_{y0} = a_{yf} = v_{yf} = 0$.

According to the findings of Hult and Tabar (2013), the reference lateral curves of vehicle, which can guarantee the succession of later acceleration and jerk minimum, can be expressed by using the fifth-order polynomial function. Considering the initial and final lateral states of vehicle, this function can be written as:

$$Y_r(t) = (Y_0 - Y_f)\left(-6\left(\frac{t}{t_f}\right)^5 + 15\left(\frac{t}{t_f}\right)^4 + 10\left(\frac{t}{t_f}\right)^3\right) + Y_0, \quad t_0 \le t \le t_f \tag{7}$$

According to equation (7), t_f can be written as:

$$t_f = \sqrt{\frac{10}{\sqrt{3}}\frac{|Y_0 - Y_1|}{|a_{y,\max}|}} \tag{8}$$

where $a_{y,\max}$ is the maximum lateral acceleration during lane change.

Moreover, insomuch as the longitudinal reference trajectory is normally longer than the lateral one, the following expression is adopted:

$$X_r(t) = X_0 + \int_{t_0}^{t} v_x dt, \quad t_0 \le t \le t_f \tag{9}$$

Figure 1 The constraints of the longitudinal and lateral forces

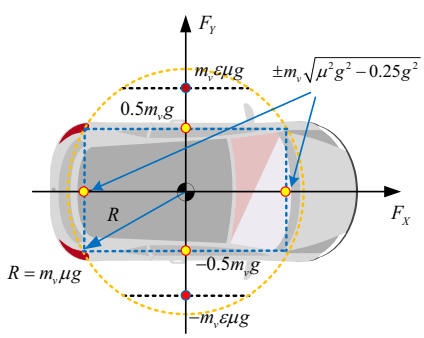

Note: The blue rectangle shows the constrained boundaries

It is noteworthy that the longitudinal acceleration is not constant. Considering the fluctuation of the longitudinal velocity in the actual steering process and the constraint of longitudinal jerk variation, the longitudinal acceleration is signified as:

$$\hat{a}_x(t) = \eta \sin(\kappa t) \tag{10}$$

where η is the positive constant and $\kappa = 2\pi/t_f$.

Equations (7)-(11) constitute the original reference trajectory that can maintain the continuity of steering and achieve the jerk minimum. To introduce vehicle dynamic restrictions, the yaw rate in ideal state is given:

$$\omega_r(t) = \frac{v_x(t)}{\rho(t)} = \frac{v_x\left(\dot{X}_r\ddot{Y}_r - \ddot{X}_r\dot{Y}_r\right)}{\sqrt{\left(\dot{X}_r^2 + \dot{Y}_r^2\right)^3}} \tag{11}$$

where $\rho(t)$ is the radius of curvature.

The maximum ω_r is denoted by $\omega_{r,\max}$. Because the initial and final states of X_r and Y_r are certain, the value of $\omega_{r,\max}$ is only connected to t_f. By restricting $a_{y,\max}$, $\omega_{r,\max}$ and $\hat{a}_x$ not outstripping the boundaries described in equations (4)-(6), the minimal lane change time t_f^* that can simultaneously fulfill the constraints of dynamics and the succession of later acceleration can be obtained. The new reference curve (X_r^*, Y_r^*) that can simultaneously pledge the vehicle stability and fulfill the jerk optimization is obtained.

Nevertheless, seeing that the order of ω_r is generally high, it is difficult to give the explicit expression about $\omega_{r,\max}$. In consequence, the t_f is hard to gain. Actually, by observing the variation in the yaw rate of the vehicle driving along some curves, it can be perceived that the positive and negative maximum values always approximately arise at the quadrate and three-quarter lane time, i.e. $t_f/4$ and $3t_f/4$ in Figure 2. Meanwhile, the maximum yaw rate $\omega_{r,\max}$ is monotone decreasing when the lane time increases. Therefore, can be represented as:

$$\omega_{r,\max} = \vartheta\min\left\{\left|\omega_r\left(\frac{t_f}{4}\right)\right|, \quad \left|\omega_r\left(\frac{3t_f}{4}\right)\right|\right\} \tag{12}$$

Figure 2 The variations in yaw rate with regard to the different lane change times t_f at 10 s, 8 s, 6 s and 4 s

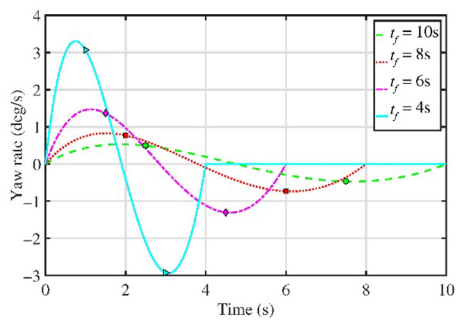

Note: The circle, square, pentagram and right-pointing triangle represent the yaw rates at $t_f/4$ and $3t_f/4$

where $\vartheta = 1.2$ is the penalty factor that offsets the loss of the authentic maximum of yaw rate. After $\omega_{r,\max}$ is gained, the bisection search algorithm is used to seek the suitable t_f. The whole search algorithm is shown in Figure 3.

3. Vehicle model for A-IWM EV

3.1 Dynamic model

In this section, as shown in Figure 4, the traditional vehicle model is used to describe the plane dynamics of A-EGV and the dynamic model can be written as:

$$\begin{aligned}
\dot{X} &= v_x\cos\theta - v_y\sin\theta \\
\dot{Y} &= v_x\sin\theta + v_y\cos\theta \\
\dot{\theta} &= \omega \\
\dot{v}_x &= \omega v_y + \left(F_X - C_a v_x^2 - C_r m_v g\right)/m_v \\
\dot{v}_y &= -\omega v_x + F_Y/m_v \\
\dot{\omega} &= M_Z/I_Z
\end{aligned} \tag{13}$$

where m_v is the IWM EV mass, I_z is the moment of inertia, X and Y are the longitudinal and lateral coordinates of vehicle in the inertial frame, θ is the heading angle of vehicle, F_X and F_Y are, respectively, the generalized longitudinal and lateral forces, M_z is the generalized external moment about the Z-axis, C_a and C_r are the aerodynamic resistance coefficient and the rolling resistance coefficient, respectively.

Figure 3 The diagram of the search algorithm to find the optimal t_f^*

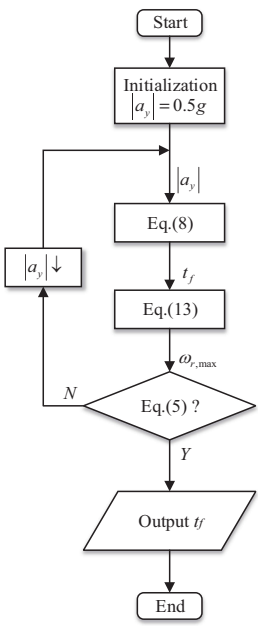

Figure 4 Schematic diagram of A-IWM EV

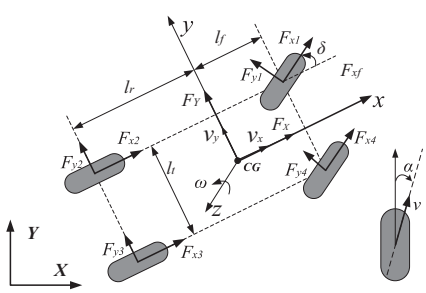

The forces F_X, F_Y and moment and M_z that are related to the four tire forces and the front steering angel δ can be expressed as:

$$\begin{aligned}
F_X &= (F_{x1}+F_{x4})\cos\delta - (F_{y1}+F_{y4})\sin\delta + F_{x2} + F_{x3} \\
F_Y &= (F_{x1}+F_{x4})\sin\delta + (F_{y1}+F_{y4})\cos\delta + F_{y2} + F_{y3} \\
M_Z &= \frac{l_t}{2}\big((F_{x4}-F_{x1})\cos\delta + (F_{y1}-F_{y4})\sin\delta \\
&\quad - F_{x2} + F_{x3}\big) - l_r(F_{y2}+F_{y3}) + l_f(F_{x1}\sin\delta \\
&\quad + F_{y1}\cos\delta + F_{x4}\sin\delta + F_{y4}\cos\delta)
\end{aligned} \tag{14}$$

In equation (14), F_{xi} and F_{yi} are, respectively, the longitudinal and lateral tire forces, where i = 1,2,3,4 represents different wheels, l_t is the track, l_f and l_r are the front and rear CM distances.

For the lateral tire force, F_{yi}, when the vehicle lateral acceleration is small and the dynamics of the tire is in the linear region, the following linear-lateral-tire-forces model can be used in vehicle control:

$$\begin{aligned}
F_{y1} &= F_{y4} = K_f\alpha_f = K_f\left(\delta - (v_y + l_f\omega)/v_x\right) \\
F_{y2} &= F_{y3} = K_r\alpha_r = K_r(l_r\omega - v_y)/v_x
\end{aligned} \tag{15}$$

where K_f and K_r are, respectively, the tire lateral stiffness, a_f and a_r are the front and rear tire slip angles. Let $\chi = [\chi_1, \chi_2, \chi_3, \chi_4, \chi_5, \chi_6]^T = [X, Y, \theta, v_x, v_y, \omega]^T$ and $u = [u_1, u_2, u_3, u_4, u_5]^T = [\delta, F_{x1}, F_{x2}, F_{x3}, F_{x4}]^T$ be the states and control inputs of system in equation (1); T is the interval, then its discrete time form can be written as

$$\chi(k+1) = \chi(k) + Tf\left(\chi(k), u(k)\right) \tag{16}$$

where f(·) represents the nonlinear terms in equation (14). Note that for the sake of expression, the discrete states and inputs at time k are written as $\chi_k = \left[\chi_1^k,\ \chi_2^k,\ \chi_3^k,\ \chi_4^k,\ \chi_5^k,\ \chi_6^k\right]^T$ and $u_k = \left[u_1^k,\ u_2^k,\ u_3^k,\ u_4^k,\ u_5^k\right]^T$.

The state trajectory, denoted by $\tilde{\chi}_{k+1}$, is obtained by applying the input $\tilde{u}_k = u_{k-1}$ to system (13) at the time k with $\tilde{\chi}_k = \chi_{k-1}$, i.e.:

$$\tilde{\chi}_{k+1} = \tilde{\chi}_k + Tf(\tilde{\chi}_k, \tilde{u}_k) \tag{17}$$

In the light of equation (17), the nonlinear system (16) can be transformed into a linear time varying (LTV) system linearized at each time step k around the point $(\tilde{\chi}_k,\ \tilde{u}_k)$ as follows:

$$\overline{\chi}_{k+1} = A_k\overline{\chi}_k + B_k\overline{u}_k + d_k \tag{18}$$

with

$$A_k = \begin{bmatrix} 1 & 0 & a_1 & T\cos\tilde{\chi}_3 & -T\sin\tilde{\chi}_3 & 0 \\ 0 & 1 & a_2 & T\sin\tilde{\chi}_3 & T\cos\tilde{\chi}_3 & 0 \\ 0 & 0 & 1 & 0 & 0 & 0 \\ 0 & 0 & 0 & a_3 & a_4 & a_5 \\ 0 & 0 & 0 & a_6 & a_7 & a_8 \\ 0 & 0 & 0 & a_9 & a_{10} & a_{11} \end{bmatrix} \tag{19a}$$

$$B_k = \begin{bmatrix} 0 & 0 & 0 & 0 & 0 \\ 0 & 0 & 0 & 0 & 0 \\ 0 & 0 & 0 & 0 & 0 \\ b_1 & \dfrac{T\cos\tilde{u}_1}{m_v} & \dfrac{T\cos\tilde{u}_1}{m_v} & \dfrac{T}{m_v} & \dfrac{T}{m_v} \\ b_2 & \dfrac{T\sin\tilde{u}_1}{m_v} & \dfrac{T\sin\tilde{u}_1}{m_v} & 0 & 0 \\ b_3 & b_4 & b_5 & -\dfrac{Tl_t}{I_Z} & \dfrac{Tl_t}{I_Z} \end{bmatrix} \tag{19b}$$

$$d_k = \tilde{\chi}_{k+1} - A_k\tilde{\chi}_k - B_k\tilde{u}_k \tag{19c}$$

where

$$a_1 = -T\left(\tilde{\chi}_5^k\cos\tilde{\chi}_3^k + \tilde{\chi}_4^k\sin\tilde{\chi}_3^k\right),$$

$$a_2 = T\left(\tilde{\chi}_4^k\cos\tilde{\chi}_3^k - \tilde{\chi}_5^k\sin\tilde{\chi}_3^k\right),$$

$$a_3 = 1 - \frac{2T}{m_v\left(\tilde{\chi}_4^k\right)^2}\left(C_a\left(\tilde{\chi}_4^k\right)^3 + K_f\sin\tilde{u}_1^k\left(\tilde{\chi}_5^k + l_f\tilde{\chi}_6^k\right)\right),$$

$$a_4 = T\tilde{\chi}_6^k + \frac{2TK_f\sin\tilde{u}_3^k}{m_v\tilde{\chi}_4^k},$$

$$a_5 = T\tilde{\chi}_5^k + \frac{2TK_fl_f\sin\tilde{u}_3^k}{m_v\tilde{\chi}_4^k},$$

$$a_6 = -\tilde{\chi}_6^kT + \frac{2T}{m_v}\left(\frac{K_r\left(\tilde{\chi}_5^k - l_r\tilde{\chi}_6^k\right)}{\left(\tilde{\chi}_4^k\right)^2} + \frac{K_f\cos\tilde{u}_1^k\left(\tilde{\chi}_5^k + l_f\tilde{\chi}_6^k\right)}{\left(\tilde{\chi}_4^k\right)^2}\right),$$

$$a_7 = 1 - \frac{2T}{m_v}\frac{\left(K_r + K_f\cos\tilde{u}_1^k\right)}{\tilde{\chi}_4^k},$$

$$a_8 = -T\tilde{\chi}_4^k + \frac{2T}{m_v}\left(\frac{K_rl_r}{\tilde{\chi}_4^k} - \frac{K_fl_f\cos\tilde{u}_1^k}{\tilde{\chi}_4^k}\right),$$

$$a_9 = -\frac{2T}{I_Z}\left(\frac{K_rl_r\left(\tilde{\chi}_5^k - l_r\tilde{\chi}_6^k\right)}{\left(\tilde{\chi}_4^k\right)^2} + \frac{K_fl_f\cos\tilde{u}_1^k\left(\tilde{\chi}_5^k + l_f\tilde{\chi}_6^k\right)}{\left(\tilde{\chi}_4^k\right)^2}\right),$$

$$a_{10} = \frac{2T}{I_Z}\left(\frac{K_rl_r}{\tilde{\chi}_4^k} - \frac{K_fl_f\cos\tilde{u}_1^k}{\tilde{\chi}_4^k}\right),$$

$$a_{11} = 1 - \frac{2T}{I_Z}\frac{\left(K_fl_f^2\cos\tilde{u}_1^k + K_rl_r^2\right)}{\tilde{\chi}_4^k},$$

$$b_1 = -\frac{T}{m_v}\left(\left(\tilde{u}_2^k + \tilde{u}_5^k\right)\sin\tilde{u}_1^k + 2K_f\left(\sin\tilde{u}_1^k + \cos\tilde{u}_1^k\left(\tilde{u}_1^k - \frac{\tilde{\chi}_5^k + l_f\tilde{\chi}_6^k}{\tilde{\chi}_4^k}\right)\right)\right),$$

$$b_2 = \frac{T}{m_v}\left(\left(\tilde{u}_2^k + \tilde{u}_5^k\right)\cos\tilde{u}_1^k + 2K_f\left(\cos\tilde{u}_1^k - \sin\tilde{u}_1^k\left(\tilde{u}_1^k - \frac{\tilde{\chi}_5^k + l_f\tilde{\chi}_6^k}{\tilde{\chi}_4^k}\right)\right)\right),$$

$$b_3 = -\frac{T}{I_Z}\left(l_t\sin\tilde{u}_1^k\left(\tilde{u}_1^k - \tilde{u}_5^k\right) + l_f\cos\tilde{u}_1^k\left(\tilde{u}_1^k + \tilde{u}_5^k\right) + 2K_fl_f\left(\cos\tilde{u}_1^k - \sin\tilde{u}_1^k\left(\tilde{u}_1^k - \frac{\tilde{\chi}_5^k + l_f\tilde{\chi}_6^k}{\tilde{\chi}_4^k}\right)\right)\right),$$

$$b_4 = -\frac{T}{I_z}\left(l_t\cos\tilde{u}_1^k - l_f\sin\tilde{u}_1^k\right),$$

$$b_5 = \frac{T}{I_z}\left(l_t\cos\tilde{u}_1^k + l_f\sin\tilde{u}_1^k\right).$$

3.2 In-wheel motor model

In this paper, it is assumed that the brushless direct current (BLDC) IWMs are used as the actuators of the EV. The dynamic models of BLDC-IWMs in both driving and braking cases can be described as follows:

$$\mathcal{J}_{w,i}\dot{\omega}_{wi} = M_{ti} - F_{xi}R_{eff}, \quad i = 1,2,3,4 \tag{20}$$

where $\mathcal{J}_{w,i}$ is the combined rotational inertia of the wheel and IWM, is the yaw rate of wheel, M_{ti} is the drive torque and R_{eff} is the effective radius of the tire.

The efficiency of adopted DC motors in the driving and braking statuses are obtained by IWMs EV tests that are conducted on a twin-roll chassis dynamometer (shown in Figure 5). Note that in the IWMs EV tests, the in-wheel motor torque values at different speeds and torque control signals were measured by a torque sensor equipped on the chassis dynamometer, and the motor control signals were changed from 1.5 V to 4.5 V with a 0.15-V step at different motor speeds. A dSPACE MicroAutoBox was used to control and record all the EGV and chassis dynamometer signals in real-time. Given the limited space available, the detailed test process is omitted in this paper, but the similar test method can be seen in (Wang *et al.*, 2011). Based on the test data, the efficiency maps are plotted in Figure 6. In addition, to introduce the motor efficiency into the efficiency management control, similar to (Chen and Wang, 2014), the polynomial fitting

Figure 5 IWMs EV chassis dynamometer test setup

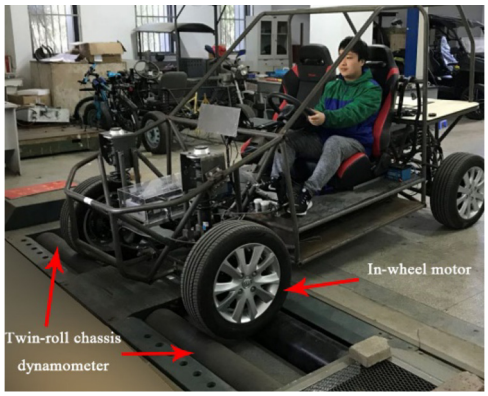

Figure 6 Driving and braking efficiency map of the DC in-wheel motors

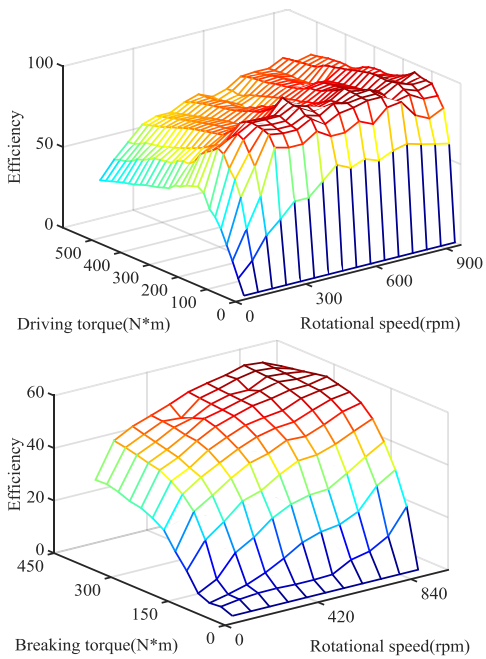

method is used to gain the change in motor efficiency, and the polynomial function can be written as follows:

$$\eta_D(M_t) = a_0 M_t{}^5 + a_1 M_t{}^4 + a_2 M_t{}^3 + a_3 M_t{}^2 + a_4 M_t + a_5$$
$$\eta_B(M_t') = b_0 M_t'{}^3 + b_1 M_t'{}^2 + b_2 M_t' + b_3 \quad (21)$$

where $\eta_D(M_t)$ and $\eta_B(M_t')$ are, respectively, the driving and braking efficiencies of one IWM, and M_t and M_t', respectively, represent the driving torque and regenerative braking torque of wheel.

4. The establishment of controller

In light of the obtained reference trajectory and vehicle model, in this section, a novel autonomous lane change control system that can ensure precise dynamic tracking control and optimal energy consumption is proposed. The structure of the control system is shown in Figure 7.

Note that different from the previous control allocation (CA) researches wherein the sliding mode control (SMC) is adopted to gain the virtual control laws (Song *et al.*, 2015), in the dynamic control level of this controller, MPC method is used to acquire the real control signals to resolve the chattering phenomena and the problem of control inputs under restraints in traditional SMC-based CA studies.

4.1 Planning control level

Based on reference trajectory in Equations (7) and (10) and t_f^* in Subsection 2.2, the reference states of vehicle in the next N_p times can be described as

$$\chi_{r,N_P} = \left[\chi_r(t_0 + kT, t_f^*), \mathrm{L}, \chi_r\left(t_0 + (k+N_P)T, t_f^*\right)\right] \quad (22)$$

where $\chi_r = \left[\mathrm{X_r},\ \mathrm{Y_r},\ \theta_r,\ \mathrm{v_{xr}},\ \mathrm{v_{yr}},\ \omega_r\right]^{\mathrm{T}}$.

Within equation (22), the reference yaw angle, longitudinal and lateral velocities can be expressed as

$$v_{xr}\left(t_0 + (k+i)T, t_f^*\right) = v_{x0} + \int_0^{t_0+(k+i)T} \hat{a}_x\left(t, t_f^*\right)dt$$
$$v_{yr}\left(t_0 + (k+i)T, t_f^*\right) = \mathbf{0}^{1\times N_P}$$

Figure 7 Structure of the proposed control system

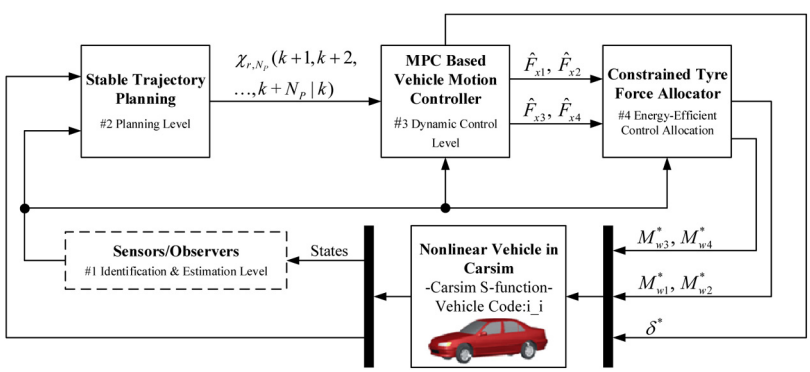

$$\theta_r\left(t_0+(k+i)T,t_f^*\right)=\arctan\left(\frac{v_{yr}\left(t_0+(k+i)T,t_f^*\right)}{v_{xr}\left(t_0+(k+i)T,t_f^*\right)}\right) \tag{23}$$

where $\mathbf{0}^{1\times Np}$ represents the zero vector that includes N_p elements, and $i=1,\ldots,N_P$.

Remark 1: *In stability control of vehicle steering, the slip angle of vehicle is expected to be zero. Because vehicle slip angle equals to the specific value of later velocity to longitudinal speed, the reference lateral speed v_{yr} is zero in equation (23).*

4.2 Dynamic control level

Based on the reference states generated by planning controller and the LTV system of vehicle (18), the cost function in the finite horizon optimal control problem can be expressed as

$$\mathcal{J}_1\sum_{i=1}^{N_P}\|\overline{\chi}_{k+i|k}-\chi_{r,k+i|k}\|^2_{Q_1}+\sum_{j=1}^{N_c}\|\delta\overline{u}_{k+j|k}\|^2_{Q_2} \tag{24}$$

where $Q_1\in R^{6\times 6}$ and $Q_2\in R^{5\times 5}$ are definite positive matrices and Z_p is control horizons. At each time step T, the following finite horizon optimal control problem is solved:

$$\min_{\Xi}\mathcal{J}_1 \tag{25}$$

$$\begin{aligned}
&s.t.\ \overline{\chi}_{t+i|k}=A_k\overline{\chi}_{t|k}+B_k\overline{u}_{s\,|k}+d_k\\
&d_k=\tilde{\chi}_{k+1}-A_k\tilde{\chi}_k-B_k\tilde{u}_k\\
&\tilde{u}_k=u_{k-1},\ \tilde{\chi}_k=\chi_k\\
&u_{k|k}=u(k-1)+\delta\overline{u}_{s|k},\ s=0,\ldots,N_c-1\\
&\delta\overline{u}_{s|k}=0,\ s=t+Z_P,\ldots,t+N_P\\
&u_{\min}\le u_{s|k}\le u_{\max}\\
&\delta u_{\min}\le\delta\overline{u}_{s|k}\le\delta u_{\max}\\
&\alpha_{j|\min}\le\alpha_{j,t|k}\le\alpha_{j|\max}
\end{aligned} \tag{26}$$

where $\Xi=[\delta\overline{u}_{s|k},\ \cdots,\delta\overline{u}_{k+N_c-1|k}]^{\mathrm{T}}$.

The optimization problem (25) can be modified into a quadratic program (QP). The sequence of optimal input deviations computed at time k by solving (25) for the current states $\chi(k)$ is denoted by Ξ^*. Then, the first sample of Ξ^* is used to compute the optimal control action and the resulting state feedback control law is

$$u_k=u_{k-1}+\delta\overline{u}^*{}_{k|k} \tag{27}$$

At the next time step $k+1$, the optimization problem (28) is solved over a shifted horizon based on the new measurements of the state $\chi(k+1)$ and based on an updated linear model in equations (18)-(19) computed by linearizing the nonlinear vehicle model.

4.3 Energy-efficient control allocation level

In Subsection 4.2, the obtained control law can only guarantee dynamic characteristics of vehicle. To reduce energy consumption, the EECA is used.

According to equation (14), the virtual control (force signals) in this paper can be expressed as

$$V_{inp}(k)=\begin{bmatrix}V_1(k)\\V_2(k)\\V_3(k)\end{bmatrix}=\begin{bmatrix}\left(F_{x1}^k+F_{x4}^k\right)\cos\delta^k+F_{x2}^k+F_{x3}^k\\\left(F_{x1}^k+F_{x4}^k\right)\sin\delta^k\\\frac{l_t}{2}\left(\left(F_{x4}^k-F_{x1}^k\right)\cos\delta^k-F_{x2}^k+F_{x3}^k\right)\\+l_f\left(F_{x1}^k\sin\delta^k+F_{x4}^k\sin\delta^k\right)\end{bmatrix} \tag{28}$$

Let $u_k=[\hat{\delta}k,\ \hat{F}_{x1}k,\ \hat{F}_{x2}k,\ \hat{F}_{x3}k,\ \hat{F}_{x4}k]$, by substituting it into above equation, then the ideal virtual control forces $V_{inp}^d(k)$ can be gained. Furthermore, based on the IWM model (20), $V_{inp}(k)$ can be re-expressed as

$$V_{inp}(k)=B_E\Lambda+B_{\mathcal{J}}w \tag{29}$$

where

$$B_E=\begin{bmatrix}\frac{\cos\hat{\delta}^k}{R_{eff}}&\frac{\cos\hat{\delta}^k}{R_{eff}}&1&1\\\frac{\sin\hat{\delta}^k}{R_{eff}}&\frac{\sin\hat{\delta}^k}{R_{eff}}&0&0\\\frac{l_f\sin\hat{\delta}^k-0.5l_t\cos\hat{\delta}^k}{R_{eff}}&\frac{l_f\sin\hat{\delta}^k+0.5l_t\cos\hat{\delta}^k}{R_{eff}}&\frac{-0.5l_t}{R_{eff}}&\frac{0.5l_t}{R_{eff}}\end{bmatrix},$$

$$B_{\mathcal{J}}=\begin{bmatrix}\frac{-\mathcal{J}_{w1}\cos\hat{\delta}^k}{R_{eff}}&\frac{-\mathcal{J}_{w2}\cos\hat{\delta}^k}{R_{eff}}&\frac{-\mathcal{J}_{w3}}{R_{eff}}&\frac{-\mathcal{J}_{w4}}{R_{eff}}\\\frac{-\mathcal{J}_{w1}\sin\hat{\delta}^k}{R_{eff}}&\frac{-\mathcal{J}_{w2}\sin\hat{\delta}^k}{R_{eff}}&0&0\\\frac{-\mathcal{J}_{w1}\left(l_f\sin\hat{\delta}^k-0.5l_t\cos\hat{\delta}^k\right)}{R_{eff}}&\frac{-\mathcal{J}_{w2}\left(l_f\sin\hat{\delta}^k+0.5l_t\cos\hat{\delta}^k\right)}{R_{eff}}&\frac{0.5\mathcal{J}_{w3}l_t}{R_{eff}}&\frac{0.5\mathcal{J}_{w4}l_t}{R_{eff}}\end{bmatrix},$$

$$\Lambda=\begin{bmatrix}M_{t1}&M_{t2}&M_{t3}&M_{t4}\end{bmatrix}^T,$$

$$w=\begin{bmatrix}\dot{\omega}_{w1}&\dot{\omega}_{w2}&\dot{\omega}_{w3}&\dot{\omega}_{w4}\end{bmatrix}^T.$$

where the wheel angular acceleration ω_{wi} can be estimated through Kalman filters, just as was done in (Chen and Wang, 2012).

Based on the virtual control expression (29), the EECA design is described to solve the following nonlinear optimization problem:

$$\begin{aligned}
&\min\mathcal{J}_2=\|B_a\begin{bmatrix}\Lambda^{\mathrm{T}}&\Lambda'^{T}\end{bmatrix}^T+B_{\mathcal{J}}w-V_{inp}^d\|^2_{Q_3}+\sigma P_c\\
&s.t.\ \Lambda_{\min}\le\Lambda\le\Lambda_{\max}\\
&\Lambda'_{\min}\le\Lambda'\le\Lambda'_{\max}\\
&\Lambda_i\Lambda'_i=0,\ \ i=1,2,3,4
\end{aligned} \tag{30}$$

where $\Lambda'=\left[M'_{t1},M'_{t2},M'_{t3},M'_{t4}\right]^{\mathrm{T}}$ stand for the regenerative brake torque signals, B_a=[BE, BE], Q_3 and σ are the positive weighting factors.

Within equation (30), P_c is the total power consumption of in-wheel motors for the driving and regenerative braking modes and can be formulated as

$$P_c = \sum_{i=1}^{4} \frac{P_{Oi}(M_{ti})}{\eta_{Di}(M_{ti})} - \sum_{i=1}^{4} P_{Ii}(M'_{ti})\,\eta_{Bi}(M'_{ti}) \tag{31}$$

where P_{Oi} and P_{Ii} is the energy consumption of IWMs in the driving model and regenerative braking mode, respectively. The corresponding electric efficiencies are indicated by η_{Di} and η_{Bi}, which can be obtained by using equation (21).

What is noteworthy is that $\mathcal{J}_2$ is nonlinear and nonconvex optimization problem. To resolve this problem, the KKT-based method, which can transfer the nonlinear/nonconvex optimization problem into an algebraic eigenvalue problem and improve the computational speed, is applied in this paper. Because the focus of this paper is not on the optimization solution, the relevant resolving approach, which can be found in (Chen and Wang, 2012), is omitted.

5. Simulation and results

To verify the capability of the proposed control system, simulation analyses is carried out. The simulations are implemented based on the CarSim-Simulink platform with a high-fidelity and full-vehicle model. The simulation parameters are listed in Table I.

The simulation results are shown in Figures 8-17. In those figures, "Dynamic" means that only dynamic tracking control is involved, "D-EFCA" signifies the controller proposed in Section 4, "E_m ", "E_θ", "E_{vx}", "E_ω" are the absolute tracking errors of actual output of Carsim to the references. And the root-mean-square-errors (RMSE) of the vehicle states tracking are listed in Table II. From Figures 8-11 and Table II, one can see that both "Dynamic" and "D-EECA" controllers can track the references accurately. Meanwhile, when searching the optimal lane time t_f, by introducing the vehicle dynamic stability boundaries into the path planning, the variations of yaw rate, lateral and longitudinal accelerations are limited (Figures 11, 16 and 17), and the homologous optimal lane time t_f^*, maximal lateral acceleration $|a_{y,\max}|$ and maximal yaw rate $|\omega_{\max}|$ are equal to 2.9 s, 0.2256 g and 4.36 deg/s, respectively.

To control energy efficiency by redistributing the torques of the four wheels (Figures 14 and 15), the power consumption in "D-EECA" should be obviously less than that in "Dynamic" as shown in Figure 12. The total energy consumption in "D-EECA" and "Dynamic" are 1.1646e + 3 kJ and 1.217e + 3 kJ during simulation (Table III). The energy is reduced by 4.3 per cent in "D-EECA", compared with "Dynamic". Insomuch as "D-EECA" controller can realize accurate dynamic tracking control and reduce energy consumption, the proposed control method is valid.

It also should be noticed that the torques of thewheel in "D-EECA" and "Dynamic" are approximated in the first half of lane change time. This phenomenon is caused because of the small weight σ. Because the dynamics performance is the first thing that must be satisfied for an autonomous vehicle, a small σ can realize the fact that the energy consumption can be reduced effectively in the case of high tracking accuracy. To further decrease energy consumption, the new EECA method and a more complete and accurate model of energy loss may be available and will be researched in the future.

Figure 8 The position of A-IWMs EV and tracking errors

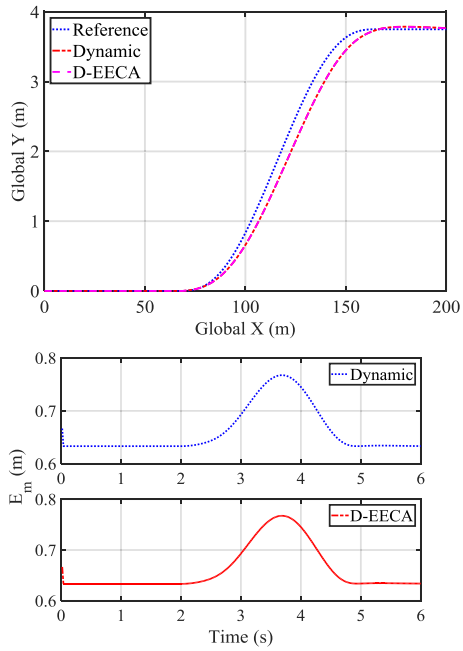

Table I Simulation parameters

Symbol	Value	Symbol	Value	Symbol	Value	Symbol	Value
m_v	1795 kg	K_r	55000 N/rad	a_0	−3.77e-9	b_0	2.49e-6
I_z	4175 kg.m^2	C_a	0.7446	a_1	7.09e-7	b_1	−4.41e-4
l_t	1.5 m	C_r	0.034	a_2	−3.75e-5	b_2	2.67e-2
l_f	1.4 m	η	2 m/s^2	a_3	−1.69e-4	b_3	1.42e-2
l_r	1.6 m	R_{eff}	0.353 m	a_4	5.22e-2	I_{wi}	0.9 kg.m^2
K_f	55,000 N/rad	σ	5	a_5	−3.35e-2	N_p	6
$M_{ti,\min}$	−45 N.m	$M'_{ti,min}$	−45 N.m	ϑ	1.2	$\delta\mu_{1,\min}$	−1 deg
$M_{ti,\max}$	45 N.m	$M'_{ti,max}$	45 N.m	$\alpha_{j\|\min}$	−4 deg	$\delta\mu_{1,\max}$	1 deg
$\delta\mu_{j,\min}$	−150 N	$\delta\mu_{j,\max}$	150 N	$\alpha_{j\|\max}$	4 deg	N_c	4
T	0.05 s	Y_0	0 m	Y_1	3.5 m	X_0	0 m
t_0	2 s	v_{x0}	120 km/h	μ	0.85	ε	0.85

Figure 9 The heading angle of A-IWMs EV and tracking errors

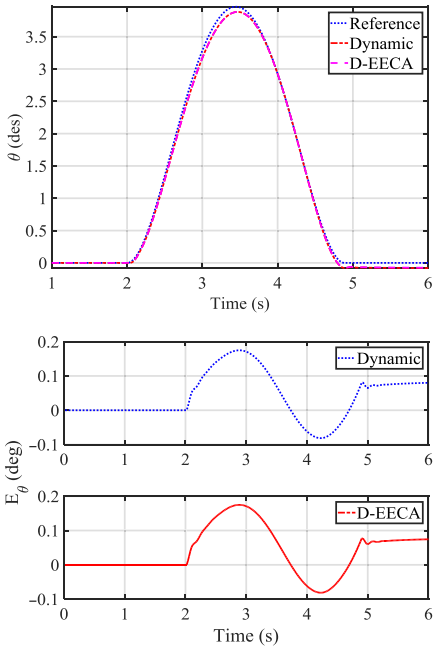

Figure 10 The longitudinal velocity of A-IWMs EV and tracking errors

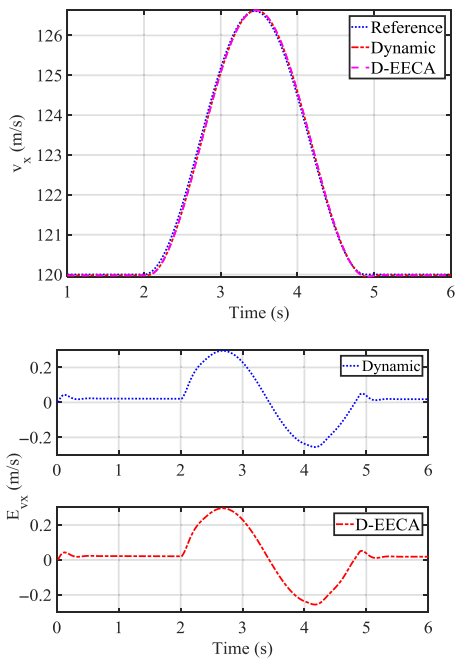

6. Conclusion

In this paper, a novel lane change control system for A-IWM EV that can enhance vehicle stability and reduce energy expenditure is proposed. The whole control system consists of stable trajectory planning level, high dynamic control level and low EECA level. In the planning level, to ensure the feasibility

Figure 11 The yaw rate of A-IWMs EV and tracking errors

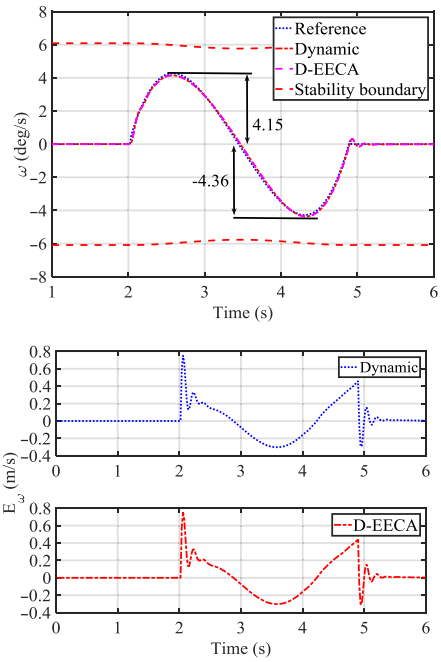

Figure 12 The power consumption of A-IWMs EV

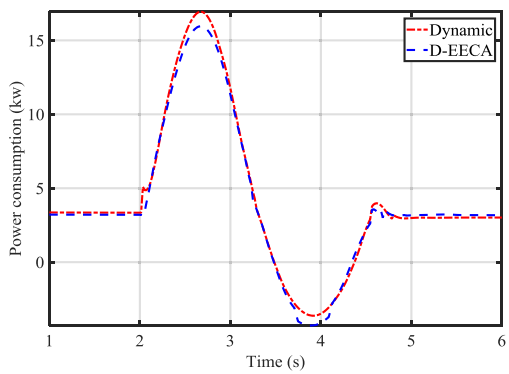

Figure 13 The steering angle of the front wheel

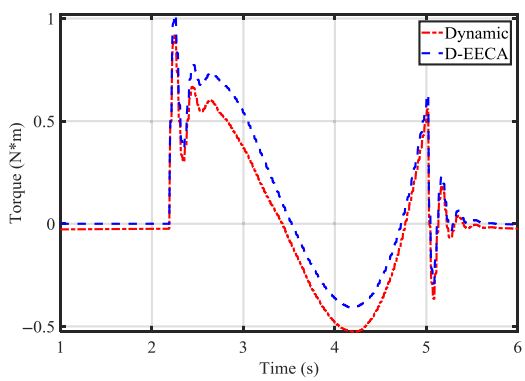

Figure 14 The torque inputs in Dynamic

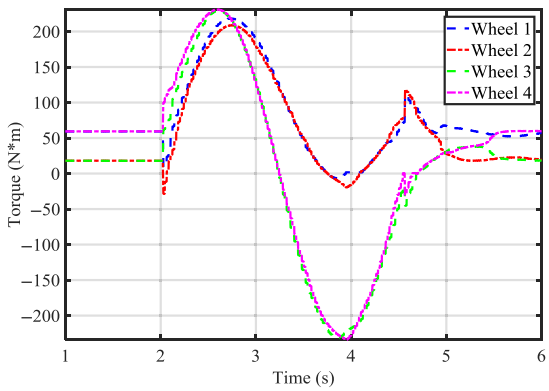

Figure 15 The torque inputs in D-EECA

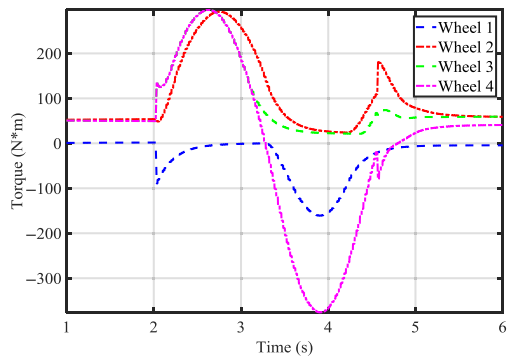

Figure 16 The longitudinal acceleration

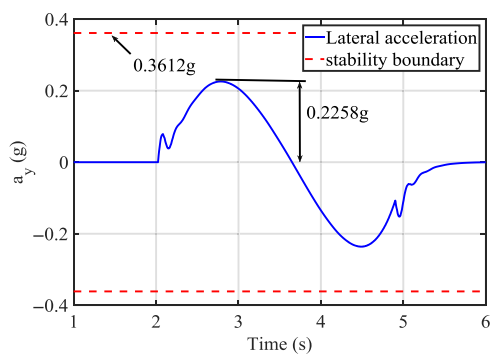

of the generated reference path, vehicle dynamics is considered and stability boundaries are established. The MPC and KKT-based algorithm are adopted to guarantee the precision of dynamic tracking and resolve the nonlinear optimization problem in the high and low levels, respectively. Simulation results on an autonomous vehicle with in-wheel motors based on a full-vehicle model in CarSim show the effectiveness of the proposed control system.

Figure 17 The lateral acceleration

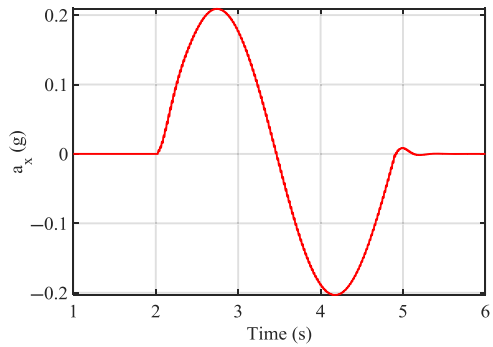

Table II RMSE of States tracking of vehicle

Controller	Path	θ	v_x	v_y	ω
"Dynamic"	0.1353	4.0267e − 4	4.0949e − 4	0.0373	5.56e − 3
"D-EECA"	0.1323	4.0073e − 4	2.3179e − 4	0.0384	2.9e − 3

Table III Total energy consumptions

Controller	Total energy (kJ)	Energy saving (%)
"Dynamic"	1.217e +3	4.3
"D-EECA"	1.1646e+3	

References

Bayar, G. (2013), "Long distance autonomous trajectory tracking for an orchard vehicle", *Industrial Robot: An International Journal*, Vol. 40 No. 1, pp. 27-40.

Berntorp, K., Olofsson, B., Lundahl, K. and Nielsen, L. (2014), "Models and methodology for optimal trajectory generation in safety-critical road-vehicle maneuvers", *Vehicle System Dynamics*, Vol. 52 No. 10, pp. 1304-1332.

Chen, C., He, Y., Bu, C., Han, J. and Zhang, X. (2014), "Quartic bezier curve based trajectory generation for autonomous vehicles with curvature and velocity constraints", *Robotics and Automation (ICRA) in 2014 IEEE International Conference in Hong Kong, China, IEEE, New York, NY*, pp. 6108-6113.

Chen, Y. and Wang, J. (2012), "Design and evaluation on electric differentials for overactuated electric ground vehicles with four independent in-wheel motors", *IEEE Transactions on Vehicular Technology*, Vol. 61 No. 4, pp. 1534-1542.

Chen, Y. and Wang, J. (2014), "Design and experimental evaluations on energy efficient control allocation methods for overactuated electric vehicles: longitudinal motion case", *IEEE/ASME Transactions on Mechatronics*, Vol. 19 No. 2, pp. 538-548.

Dai, Y., Luo, Y., Chu, W. and Li, K. (2014), "Optimum tyre force distribution for four-wheel-independent drive electric vehicle with active front steering", *International Journal of Vehicle Design*, Vol. 65 No. 4, pp. 336-359.

Hult, R. and Tabar, R.S. (2013), *Path Planning for Highly Automated Vehicles*, Chalmers University of Technology, Gothenburg.

Jin, X., Yin, G. and Chen, N. (2015), "Gain-scheduled robust control for lateral stability of four-wheel-independent-drive electric vehicles via linear parameter-varying technique", *Mechatronics*, Vol. 30, pp. 286-296.

Kim, S., Oh, H., Suk, J. and Tsourdos, A. (2014), "Coordinated trajectory planning for efficient communication relay using multiple UAVs", *Control Engineering Practice*, Vol. 29, pp. 42-49.

Li, B., Du, H. and Li, W. (2017), "A potential field Approach-Based trajectory control for autonomous electric vehicles with in-Wheel Motors", *IEEE Transactions on Intelligent Transportation Systems*, Vol. 18 No. 8, pp. 2044-2055.

Li, D., Song, Y., Huang, D. and Chen, H. (2013), "Model-independent adaptive fault-tolerant output tracking control of 4WS4WD road vehicles", *IEEE Transactions on Intelligent Transportation Systems*, Vol. 14 No. 1, pp. 169-179.

Naranjo, J.E., Gonzalez, C., Garcia, R. and De Pedro, T. (2008), "Lane-change fuzzy control in autonomous vehicles for the overtaking maneuver", *IEEE Transactions on Intelligent Transportation Systems*, Vol. 9 No. 3, pp. 438-450.

Potluri, R. and Singh, A.K. (2015), "Path-tracking control of an autonomous 4WS4WD electric vehicle using its natural feedback loops", *IEEE Transactions on Control Systems Technology*, Vol. 23 No. 5, pp. 2053-2062.

Rajamani, R. (2011), *Vehicle Dynamics and Control*, Springer Science & Business Media, Dordrecht.

Song, P., Tomizuka, M. and Zong, C. (2015), "A novel integrated chassis controller for full drive-by-wire vehicles", *Vehicle System Dynamics*, Vol. 53 No. 2, pp. 215-236.

Soudbakhsh, D., Eskandarian, A. and Chichka, D. (2013), "Vehicle collision avoidance maneuvers with limited lateral acceleration using optimal trajectory control", *Journal of Dynamic Systems, Measurement, and Control*, Vol. 135 No. 4, p. 41006.

Wang, J., Wu, J., Zheng, X., Ni, D. and Li, K. (2016), "Driving safety field theory modeling and its application in pre-collision warning system", *Transportation Research Part C: Emerging Technologies*, Vol. 72, pp. 306-324.

Wang, J., Zhang, L., Zhang, D. and Li, K. (2013), "An adaptive longitudinal driving assistance system based on driver characteristics", *IEEE Transactions on Intelligent Transportation Systems*, Vol. 14 No. 1, pp. 1-12.

Wang, J.Q., Li, S.E., Zheng, Y. and Lu, X.Y. (2015), "Longitudinal collision mitigation via coordinated braking of multiple vehicles using model predictive control", *Integrated Computer-Aided Engineering*, Vol. 22 No. 2, pp. 171-185.

Wang, R., Chen, Y., Feng, D., Huang, X. and Wang, J. (2011), "Development and performance characterization of an electric ground vehicle with independently actuated in-wheel motors", *Journal of Power Sources*, Vol. 196 No. 8, pp. 3962-3971.

Wu, F.K., Yeh, T.J. and Huang, C.F. (2013), "Motor control and torque coordination of an electric vehicle actuated by two in-wheel motors", *Mechatronics*, Vol. 23 No. 1, pp. 46-60.

Yin, G., Wang, R. and Wang, J. (2015), "Robust control for four wheel Independently-Actuated electric ground vehicles by external Yaw-Moment generation", *International Journal of Automotive Technology*, Vol. 16 No. 5, pp. 839-847.

You, F., Zhang, R., Lie, G., Wang, H., Wen, H. and Xu, J. (2015), "Trajectory planning and tracking control for autonomous lane change maneuver based on the cooperative vehicle infrastructure system", *Expert Systems with Applications*, Vol. 42 No. 14, pp. 5932-5946.

Corresponding author

Guodong Yin can be contacted at: ygd@seu.edu.cn